Journal of Nuclear Science and Technology

ISSN: 0022-3131 (Print) 1881-1248 (Online) Journal homepage: https://www.tandfonline.com/loi/tnst20

Modelling and Simulation of Reactor Fuel Cladding under Loss-of-Coolant Accident Conditions

Tero MANNGÅRD & Ali R. MASSIH

To cite this article: Tero MANNGÅRD & Ali R. MASSIH (2011) Modelling and Simulation of Reactor Fuel Cladding under Loss-of-Coolant Accident Conditions, Journal of Nuclear Science and Technology, 48:1, 39-49, DOI: 10.1080/18811248.2011.9711677

To link to this article: https://doi.org/10.1080/18811248.2011.9711677

Journal of NUCLEAR SCIENCE and TECHNOLOGY, Vol. 48, No. 1, p. 39–49 (2011)

ARTICLE

Modelling and Simulation of Reactor Fuel Cladding under Loss-of-Coolant Accident Conditions

Tero MANNGÅRD[1] and Ali R. MASSIH[1,2,*]

[1]*Quantum Technologies AB, Uppsala Science Park, SE-75183, Sweden*
[2]*Malmö University, SE-20506 Malmö, Sweden*

(Received January 28, 2010 and accepted in revised form July 14, 2010)

We present a unified model for calculation of zirconium alloy fuel cladding rupture during a postulated loss-of-coolant accident in light water reactors. The model treats the Zr alloy solid-to-solid phase transformation kinetics, cladding creep deformation, oxidation, and rupture as functions of temperature and time in an integrated fashion during the transient. The fuel cladding material considered here is Zircaloy-4, for which material property data (model parameters) are taken from the literature. We have modelled and simulated single-rod transient burst tests in which the rod internal pressure and the heating rate were kept constant during each test. The results are compared with experimental data on cladding rupture strain, temperature, and pressure. The agreement between computations and measurements in general is satisfactory. The effects of heating rate and rod internal pressure on the rupture strain are evaluated on the basis of systematic parameter variations of these quantities. In the α-phase of Zr, the burst strain decreases with increasing heating rate, whereas in the two-phase coexistence ($\alpha + \beta$) domain and β-phase, the situation is more complex. Also, the mechanism for creep deformation in the ($\alpha + \beta$) domain is not well understood; hence, its mechanistic constitutive relation is presently unknown.

KEYWORDS: LOCA, fuel cladding, creep, rupture, modelling

I. Introduction

In a postulated loss-of-coolant accident (LOCA) in light-water reactors (LWRs), zirconium alloy fuel claddings are subjected to high temperatures (700–1,500 K) and internal pressures. These can cause excessive deformation (ballooning), which may eventually lead to rupture of cladding following the accident. The cladding tube hoop (tangential) strain at failure determines whether rod-to-rod contact would occur in a fuel assembly. Moreover, it would decide the degree of coolant blockage in the refilling and flooding phase of LOCA.[1,2)]

In the LOCA safety analysis (required for the licensing of a reactor fuel system), a failure criterion model is needed to predict the temperature and time at which cladding ruptures, and also the total hoop strain at, or close to, the location of rupture. The physical behaviour of cladding during the accident is governed by phase transformation, oxidation, creep deformation, and rupture of zirconium alloy within a time scale of about 120 s. The objective of this note is to delineate a unified generic computational method to account for these phenomena based on empirically attained material property data reported in the literature. We synthesise the previously described kinetics of zirconium alloy phase transformation[3)] with the equations for cladding creep, oxidation, and burst[4,5)] to calculate the rupture time/temperature during a transient.

In our study, we evaluate the behaviour of Zircaloy-4 fuel cladding tube with nominal chemical composition: Zr-base, 1.5Sn-0.2Fe-0.1Cr-0.12O by wt%. Zirconium alloys in solid state undergo a phase transformation from the low-temperature hexagonal closed-packed (hcp) α-phase to body-centred cubic (bcc) β-phase.[6)] Solid-state phase equilibria of Zircaloy-4 have been investigated experimentally by Miquet *et al.*,[7)] who reported the prevalence of four phase domains: ($\alpha + \chi$) up to 1,081 K, ($\alpha + \beta + \chi$) from 1,081 to 1,118 K, ($\alpha + \beta$) between 1,118 and 1,281 K, and β-phase above 1,281 K. Here, χ refers to the intermetallic hexagonal Laves phase $Zr(Fe,Cr)_2$; see, for example, Ref. 8). For the sake of illustration, we have depicted an *isopethal* (constant composition) section of Zircaloy-4 with only the oxygen concentration as a variable in **Fig. 1**. A short survey of the literature on zirconium alloy phase transformation behaviour was presented in our previous paper.[3)]

Similar past modelling approaches comprise the works presented in Refs. 4) and 5), which however, did not include a phase transformation kinetics model. More recent modelling efforts are the works of Forgeron *et al.*[12)] and Brachet *et al.*[13)] and the implementation of such models in a fuel performance code.[11)] Although our general modelling approach is similar to that presented in Refs. 12) and 13), our basic equations for phase transformation kinetics, combined

*Corresponding author, E-mail: alma@quantumtech.se

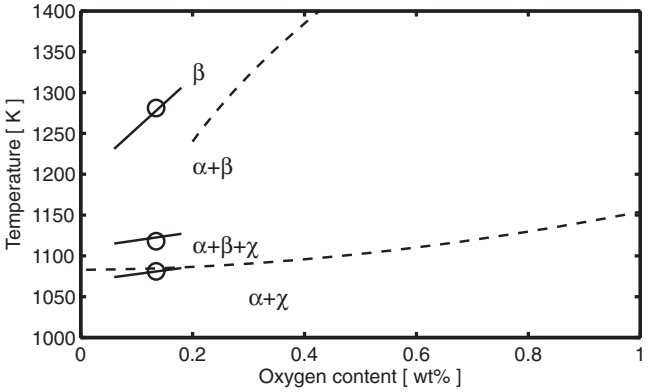

Fig. 1 An isopethal section of Zircaloy-4 versus oxygen concentration. The open circles are the temperature levels for the Zircaloy-4 (oxygen content of 0.135 wt%) determined by Miquet *et al.*[7] The short solid lines through the open circles show the measured temperatures within a narrow range of oxygen concentration studied by Miquet *et al.*[9] The dashed lines are the empirical correlations provided by Chung and Kassner[10] pertinent to LOCA conditions. The regions for the coexistent phases $(\alpha + \chi)$ and $(\alpha + \beta + \chi)$ are indicated in the figure, where χ refers to the second phase precipitate $Zr(Cr,Fe)_2$ in the alloy.

creep and oxidation equations, and mechanical equilibrium are different. In addition, we provide the numerical details of our computations, which have an impact on the results, and are usually lacking in the open literature.

The organisation of this paper is as follows. Section II presents the model and the basic equations used for phase transformation, creep, oxidation, and cladding burst. Sample computations, simulating transient single-rod burst experiment in which the heating rate and rod pressure were kept constant in each test, are presented in Sec. III. Section III also includes comparisons between model computations and experimental data, plus parametric studies using the integrated model. In Sec. IV, we discuss the limitations and applicability of the submodels utilised, and Sec. V concludes the report.

II. Governing Equations

The present method considers a set of three differential equations for describing the kinetics of phase transformation, the creep deformation, and oxidation of zirconium alloys. The latter two equations are numerically solved simultaneously, while the solutions of the phase transformation equations provide input to the creep rate equation and the cladding burst stress-temperature relation in the two-phase coexistence $(\alpha + \beta)$ region of the Zr alloy.

The phase transformation model has been detailed in our previous articles.[3,14] It expresses the rate of the transformed volume fraction (y) according to

$$\frac{\mathrm{d}y}{\mathrm{d}t} = \frac{y_s(T) - y}{\tau_c(T)}, \tag{1}$$

where $y_s(T)$ is the equilibrium value y at temperature T, and $\tau_c(T)$ is the characteristic time of phase transformation. The expression for y_s is given as[3]

$$y_s = \frac{1}{2}\left[1 + \tanh\left(\frac{T - T_{cent}}{T_{span}}\right)\right], \tag{2}$$

where T_{cent} and T_{span} are material-specific parameters related to the centre and the span of the mixed-phase temperature region, respectively. For Zircaloy-4, we use $T_{cent} = 1{,}159\,\mathrm{K}$ and $T_{span} = 44\,\mathrm{K}$. The expression for τ_c is given in Ref. 3) for Zircaloy-4.

The steady-state creep strain rate of Zr alloy cladding is expressed by a Norton law[4,5]

$$\frac{\mathrm{d}\varepsilon_\theta}{\mathrm{d}t} = A_\theta f(x) \exp(-Q/RT)\sigma_\theta^n, \tag{3}$$

or alternatively, by a Harper-Dorn law[15] in the form

$$\frac{\mathrm{d}\varepsilon_\theta}{\mathrm{d}t} = \frac{A_\theta}{T} f(x) \exp(-Q/RT)\sigma_\theta^n, \tag{4}$$

where ε_θ and σ_θ are the hoop (tangential) strain and stress of the cladding tube, respectively, A_θ the strength coefficient, Q the activation energy, R the gas constant, T the absolute temperature, n the stress exponent, and $f(x)$ accounts for the effect of oxygen concentration x, written in the form[16]

$$f(x) \equiv \exp[B(x)]. \tag{5}$$

The creep strength coefficient A_θ, as in Ref. 5), is calculated from

$$A_\theta = \left[\frac{1}{4}(F+G) + H\right]^{(n-1)/2}\left(H + \frac{1}{2}F\right) \times (F+G)^{-(n+1)/2} A_z, \tag{6}$$

where the Hill anisotropic factors F, G, and H[17] are used in the α-phase and isotropic values of $F = G = H = 0.5$ are used for the $(\alpha + \beta)$- and β-phase domains. For the anisotropic α-Zr alloy, we assume $F = 0.956$, $G = 0.304$, and $H = 0.240$.[4] We should note that the effect of oxygen concentration x is not included in Eqs. (1) and (2) for the phase transformation.

All the parameters appearing in Eqs. (3) and (4) are described in **Tables 1** and **2** for Zircaloy-4, respectively. The strength coefficient A_θ for the Zr alloy is calculated from the corresponding uniaxial value A_z through the anisotropic factors using Hill's relation.[4,5,18] For the oxygen-dependent term, Eq. (5), we use Burton *et al.*'s empirical relation $B(x) = -342x$,[16] where $x \leq 0.015$ is the oxygen weight fraction in the α-phase of zirconium alloy. The effect of oxygen on creep in β-phase is neglected.[16,19]

For symmetrical deformations, the hoop stress (σ_θ) in a slender tube (cladding) under a differential pressure Δp can be related to the hoop strain as[20,21]

$$\sigma_\theta = \sigma_0 \exp(2\beta\varepsilon_\theta), \tag{7}$$

where $\sigma_0 = \Delta p\, r_0/w_0$, and r_0 and w_0 are the initial cladding midradius and wall thickness, respectively. In addition, $\beta = 1 + \lambda/2$, $\lambda = (G - F)/(F + 2H)$. When there are end restraints on the tube, $\beta = 1$. Thus, using Eq. (7), we write Eq. (3) as

$$\frac{\mathrm{d}\varepsilon_\theta}{\mathrm{d}t} = A_\theta f(x) \exp(-Q/RT)\sigma_0^n \exp(2n\beta\varepsilon_\theta). \tag{8}$$

Table 1 Creep law parameters for Zircaloy-4,[5] *cf.* Eq. (3)

Parameter	Unit	α-phase	β-phase	$(\alpha+\beta)$[a]
A_z	$\mathrm{MPa}^{-n}\,\mathrm{s}^{-1}$	19,400	7.9	0.24
n	—	5.89	3.78	2.33
A_θ	$\mathrm{MPa}^{-n}\,\mathrm{s}^{-1}$	1,489	3.97	0.15
Q/R	K	38,487	17,079	12,316

[a] Valid for strain rates $\leq 0.003\,\mathrm{s}^{-1}$; otherwise, linear interpolation of parameters between α and β phases is used.

Table 2 Creep law parameters for Zircaloy-4 alloy,[15] *cf.* Eq. (4)

Parameter	Unit	α-phase ($\sigma \leq 15$ MPa)	α-phase ($\sigma > 15$ MPa)
A_z	$\mathrm{KMPa}^{-n}\,\mathrm{s}^{-1}$	1.00×10^6	1.63×10^8
n	—	1.3	5.0
A_θ	$\mathrm{KMPa}^{-n}\,\mathrm{s}^{-1}$	5.04×10^5	1.80×10^7
Q/R	K	22,852	38,006
		β-phase	β-phase
A_z	$\mathrm{KMPa}^{-n}\,\mathrm{s}^{-1}$	1.00×10^4	1.00×10^4
n	—	4.25	4.25
A_θ	$\mathrm{MPa}^{-n}\,\mathrm{s}^{-1}$	4.70×10^3	4.70×10^3
Q/R	K	18,041	18,041

Assuming that oxygen will uniformly get distributed in the cladding, the oxidation rate of Zr alloy follows a parabolic law of the form

$$\frac{\mathrm{d}x}{\mathrm{d}t} = \frac{1}{2x}\eta^2, \tag{9}$$

$$\eta = 0.724\exp(-10481/T)\frac{1+\varepsilon_\theta}{w_0\rho_0}, \tag{10}$$

where ρ_0 is the Zr alloy density $\rho_0 = 6.56\,\mathrm{g\,cm}^{-3}$; Eq. (10) was found from experiments made under the assumption of isothermal steam oxidation of Zircaloy-4 cladding material within a temperature range of 973 to 1,573 K and an exposure time of ≤ 15 min.[4]

Finally, we use the relation for the rupture (burst) stress vs. temperature T and oxygen concentration x in the form[4]

$$\sigma_B = a\exp(-bT)g(x), \tag{11}$$

where a and b are material-dependent constants (**Table 3**) obtained experimentally and

$$g(x) = \exp\left[-\left(\frac{x-x_0}{0.00095}\right)^2\right]. \tag{12}$$

Here, $x_0 = 0.0012$ is the as-fabricated oxygen weight fraction of the Zr alloy.[4,5] Cladding rupture occurs when $\sigma_\theta = \sigma_B$.

The strain rate in the two-phase coexistence $(\alpha+\beta)$ region follows a separate mechanism than in the single-phase region.[22,23] For computational convenience, some authors have suggested *ad hoc* correlations in the mixed-phase region for Zircaloy-4[4,5] or have considered homogenisation according to[11,24]

Table 3 Material-dependent parameters in the burst stress *vs.* temperature, Eq. (11) for Zircaloy-4 cladding tube[4]

Parameter	Unit	α-phase	β-phase	$(\alpha+\beta)$
a	MPa	830	2,300	3,000 at $T_{\alpha\beta}$
b	K^{-1}	0.001	0.003	0.003 at $T_{\alpha\beta}$

For Zircaloy-4 according to Ref. 4), the boundary temperatures are: $T_\alpha = 1085.15 + 14.28(q)^{0.28}$ (K) with q heating rate ($\mathrm{K\,s}^{-1}$); $T_\beta = 1248.15$ (K); mid temperature of the $(\alpha+\beta)$-phase $T_{\alpha\beta} = (T_\alpha + T_\beta)/2$. Linear interpolation of $\ln a$ and b in the $(\alpha+\beta)$-phase between the temperatures T_α, $T_{\alpha\beta}$, and T_β.

$$\dot{\varepsilon}_{\alpha\beta} = \dot{\varepsilon}_\alpha(1-y) + \dot{\varepsilon}_\beta y, \tag{13}$$

or alternatively,

$$\dot{\varepsilon}_{\alpha\beta} = \dot{\varepsilon}_\alpha^{1-y}\cdot\dot{\varepsilon}_\beta^{y}, \tag{14}$$

where the dot denotes time derivative, subscripts α and β the respective phases, and y the volume fraction of the β-phase calculated from Eq. (1). Similarly, the rupture stress in the $(\alpha+\beta)$ region is calculated using an *ad hoc* correlation[4] or employing a mixing rule of the form[12]

$$\sigma_{\alpha\beta} = \sigma_\alpha^{1-y}\cdot\sigma_\beta^{y}. \tag{15}$$

III. Computations

1. Temperature History Evaluations

Let us now, using the integrated model outlined in Sec. II, calculate a sample case from single-rod transient burst tests, which were conducted within the REBEKA program using fuel rod simulators with indirect electric heating.[4] In these tests to achieve well-defined experimental boundary conditions, the internal overpressure and the heating rate were kept constant during the deformation process. **Figure 2** illustrates schematically the test procedure. The test parameters, rod overpressure and heating rate, were in the range of 1 to 14 MPa and 1 to $30\,\mathrm{K\,s}^{-1}$, respectively. The cladding tubes used were made of Zircaloy-4 with inner and outer diameters of 9.30 and 10.75 mm, respectively.[4]

In our sample computations, we use a heating rate of $10\,\mathrm{K\,s}^{-1}$ and assume rod internal overpressures of $\Delta p = 1$ and 8 MPa with restrained ends ($\beta = 1$). Zircaloy-4 cladding with the property data is presented in Table 1 and Ref. 3). The initial cladding midradius and wall thickness used in Eq. (7) are $r_0 = 5.0125$ mm and $w_0 = 0.725$ mm, respectively.

We have implemented the aforementioned governing equations and material property data in a computer program for calculating Zircaloy-4 phase transformation, cladding creep, oxidation, and burst as a function of time and temperature in tandem.

We solve Eq. (1) for a given temperature time-history using the Runge-Kutta algorithm of orders 4 and 5[25] with the initial condition $y(0) = 0$ and $T(0) = 900$ K. The results, the fraction of β-phase transformed as a function of temperature for the alloy, are presented in **Fig. 3**.

The cladding creep and oxidation Eqs. (8) and (9) are solved simultaneously using the same kind of Runge-Kutta

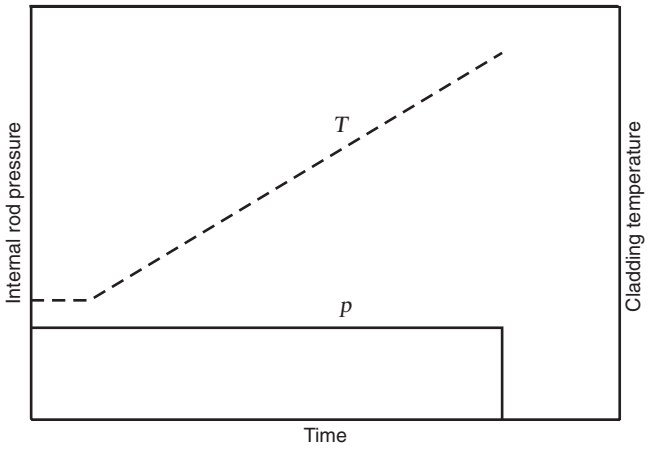

Fig. 2 Schematic of the conditions of transient single-rod burst tests performed by Erbacher *et al.*[4] in the parameter range: $\dot{T} = 1 \rightarrow 30\,\mathrm{K\,s^{-1}}$ and $p = 1 \rightarrow 14\,\mathrm{MPa}$

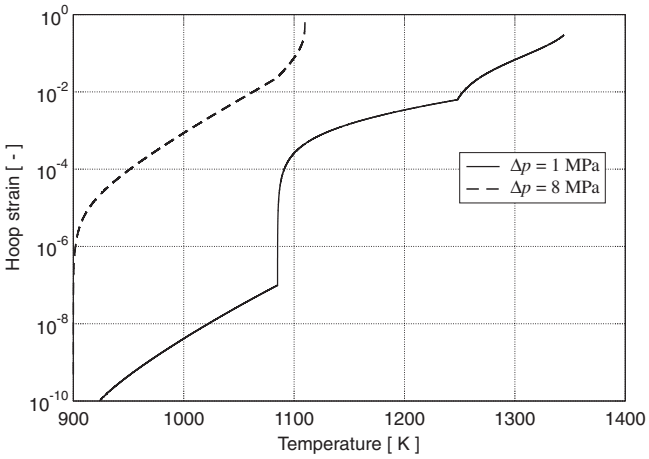

Fig. 4 Cladding hoop strain due to creep deformations versus temperature during the transient at a heating rate of $10\,\mathrm{K\,s^{-1}}$ for rod internal overpressures of 1 and 8 MPa

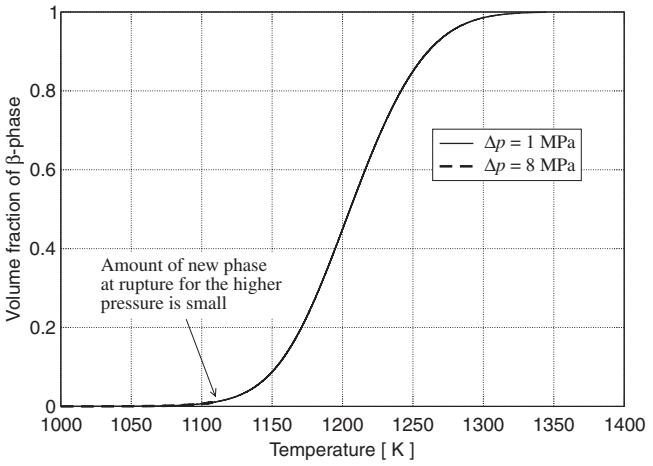

Fig. 3 Volume fraction of β-phase as a function of temperature at a heating rate of $10\,\mathrm{K\,s^{-1}}$ for rod internal overpressures of 1 and 8 MPa

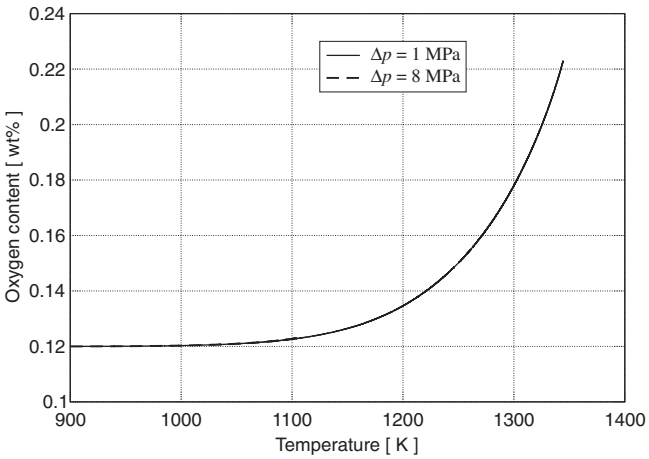

Fig. 5 Cladding oxygen weight concentration versus temperature during the transient at a heating rate of $10\,\mathrm{K\,s^{-1}}$ for rod internal overpressures of 1 and 8 MPa

algorithm (extended to a system of differential equations) with the initial conditions $\varepsilon_\theta(0) = 0$ and $x(0) = 0.0012$. In the computations presented here, we have employed Eq. (3) and Table 1 for the creep rate. For the burst stress, Eq. (11) and Table 3 were used. That is, the mixing rules given by relations (13)–(15) in the two-phase coexistence $(\alpha + \beta)$ domain for the creep rate and burst, respectively, were not utilised. The results are depicted in **Figs. 4** and **5** as a function of temperature up to the cladding failure time. The cladding burst stress versus temperature is plotted in **Fig. 6**. The calculated time, temperature, and hoop strain at the onset of cladding rupture are 44.5 s, 1,345 K, and 29.8% for $\Delta p = 1\,\mathrm{MPa}$; and 21 s, 1,110 K, and 77.3% for $\Delta p = 8\,\mathrm{MPa}$, respectively. The time step in computations was $\Delta t = 0.1\,\mathrm{ms}$.

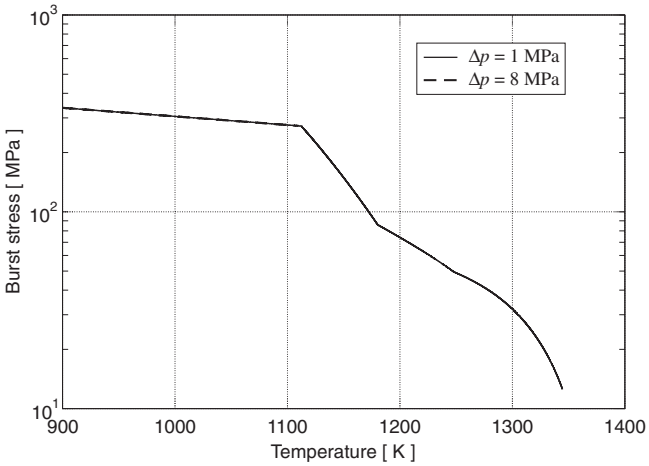

Fig. 6 Variation of burst stress with temperature during the transient at a heating rate of $10\,\mathrm{K\,s^{-1}}$ for rod internal overpressures of 1 and 8 MPa

2. Comparison with Experimental Burst Data

In this section, we compare the results of computations with a number of cladding tube rupture experiments per-

formed under pressurised water reactor LOCA conditions. The experiments considered are reported in Refs. 4) and 26–28).

As mentioned in the previous subsection, single-rod burst tests in steam were performed within the REBEKA program using fuel rod simulators with indirect electric heating and 325 mm heated length. The rod simulator comprised Al_2O_3 pellets (instead of UO_2 fuel pellets) clad with Zircaloy-4 tubing.[4,26)] The temperature history of the cladding during the test was measured using thermocouples spot-welded on the outer surface of the cladding. The deformation of cladding as a function of time was recorded by X-ray cinematography by using a high-speed camera, which allowed the observation of the cladding ballooning process during the test. Data on burst temperature, burst pressure, and burst strain are presented in Ref. 4). The heating rate in these tests ranged from 0.8 to 35 K s^{-1}.

In the Karb *et al.*[27)] experiments, the main objective was to investigate the possible influence of nuclear environment on fuel cladding failure mechanisms (see also Ref. 29)). In these experiments, both unirradiated and preirradiated PWR-type test fuel rods (with Zircaloy-4 cladding tube with inner and outer diameters of 9.30 and 10.75 mm, respectively) were subjected to temperature transients simulating the second heat-up phase of a LOCA. The nuclear environment was primarily characterised by the heat generated in UO_2 fuel and the heat transfer from the fuel to the cladding outer surface in the FR2 reactor at Karlsruhe, Germany. In addition, 8 reference samples with electrically heated rod simulators with Al_2O_3 pellets were tested in the in-pile loop under conditions identical to those of the nuclear tests.[27)]

In these tests, the burst data (temperature at rupture, rupture pressure, and rupture strain) of the nuclear fuel rods did not indicate differences from the results obtained from electrically heated fuel rod simulators, and nor did they show the effect of irradiation exposure (up to 35 MWd/kgU). In our study, we only consider the unirradiated rods and the electrically heated fuel rod simulators by prescribing temperature histories to the cladding and evaluate the burst behaviour with the aforementioned model (Sec. II). The heating rate of the unirradiated rods varied between 7 to 19 K s^{-1}, whereas that of the electrically heated rod simulators had heating rates of 12–13 K s^{-1}.

Erbacher and Leistikow[28)] have presented Zircaloy-4 burst data obtained from multirod burst tests performed within the REBEKA program. The data represent tests that had the potential for maximum ballooning, *i.e.*, burst taking place in the α-phase of Zircaloy around 800°C. The heating rate during heat-up in the tests was 7 K s^{-1}. The burst pressures in the test were between 5 and 7 MPa and the measured hoop strains ranged from 0.28 to 0.55. Moreover, the circumferential temperature gradient in the tests varied between 20 and 70 K. For further details on the burst data, see Ref. 28).

Cladding burst computations, for comparison with experimental results, are carried out by varying the constant internal overpressure in the range from 0.1 to 14 MPa (in steps of 0.1 MPa) at two different constant heating rates, 1 and 35 K s^{-1}. The same model assumptions as in the foregoing subsection are made. The resulting cladding burst curves,

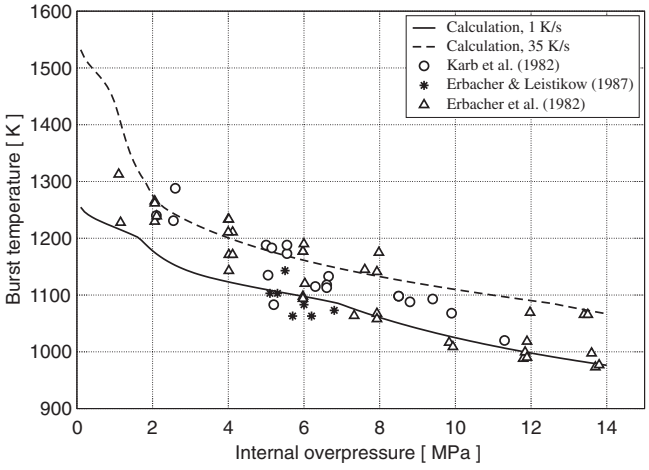

(a)

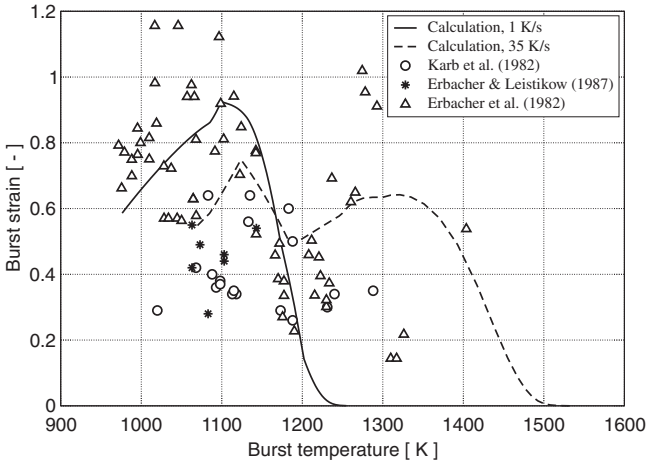

(b)

Fig. 7 Calculated burst curves for Zircaloy-4 cladding generated by varying constant internal overpressure in the range from 0.1 to 14 MPa at two different constant heating rates, 1 and 35 K s^{-1}. Creep rate is calculated according to Ref. 5) and burst stress criterion according to Ref. 4). The cladding outside diameter and wall thickness used in the calculations are 10.75 and 0.725 mm, respectively. Three sets of measured burst data[4,27,28)] are included for comparison.

calculated in this way, *i.e.*, (i) burst temperature versus internal overpressure and (ii) cladding hoop burst strain versus burst temperature, together with burst test data[4,27,28)] are plotted in **Figs. 7**(a) and 7(b), respectively. **Figure 8**(a) depicts the calculated hoop strain versus time for a load combination of internal overpressure/heating rate of 8 MPa/35 K s^{-1}. This calculation represents one point on the burst curves for 35 K s^{-1} shown in Figs. 7(a)–7(b). The final (maximum) calculated hoop strain value calculated at $\approx$6.6 s amounts to $\approx$0.694. The burst hoop strain, calculated from the burst correlation, at this instant in time is $\approx$0.718. Figure 8(b) shows that the strain increases by about 2.5% in the last 0.1 ms time step.

It has been noted by Erbacher and Leistikow[28)] that in single-rod experiments in the α-phase and the two-phase coexistence ($\alpha + \beta$) domain of Zircaloy-4 tube, there is a direct relationship between the hoop burst strain and the

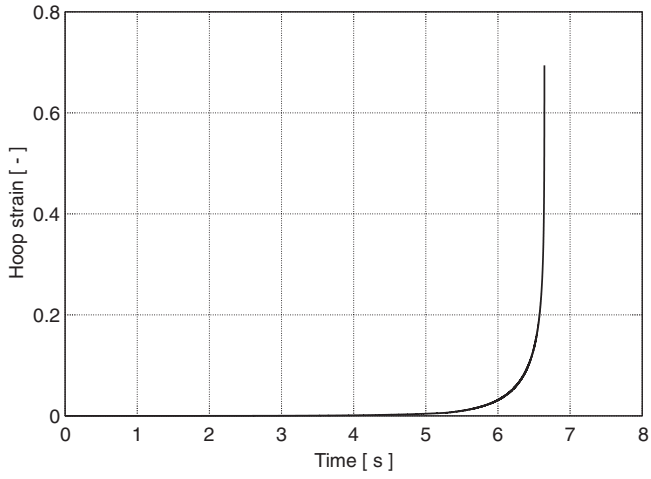

(a)

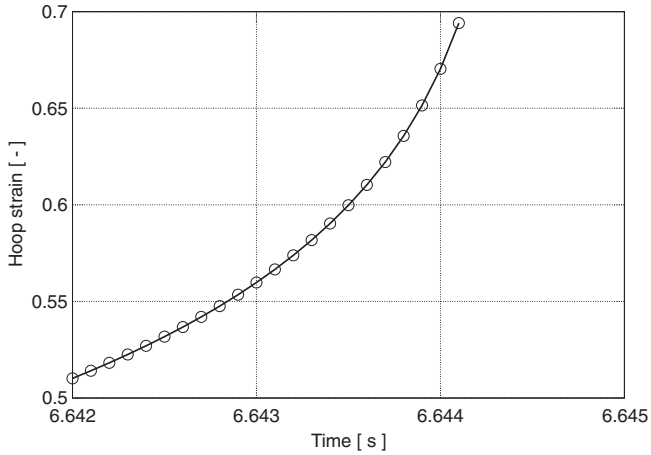

(b)

Fig. 8 (a) Hoop strain as a function of time, calculated for a heating rate of 35 K s^{-1} and internal overpressure of 8 MPa, until the instant of cladding burst. (b) A closeup of the hoop strain for the last 2 ms before cladding burst. The ring symbols mark calculated time intervals.

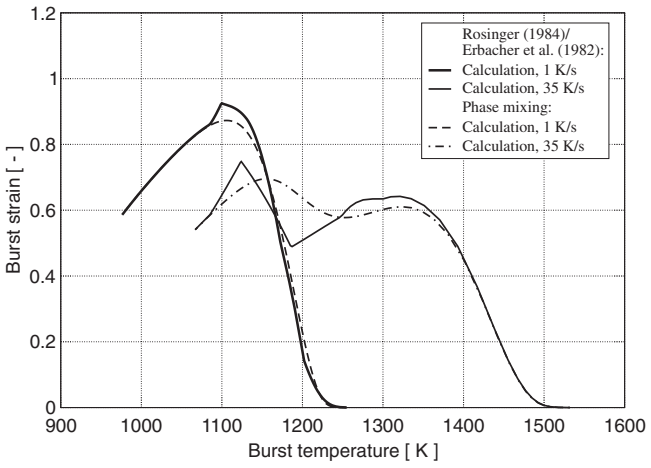

(a)

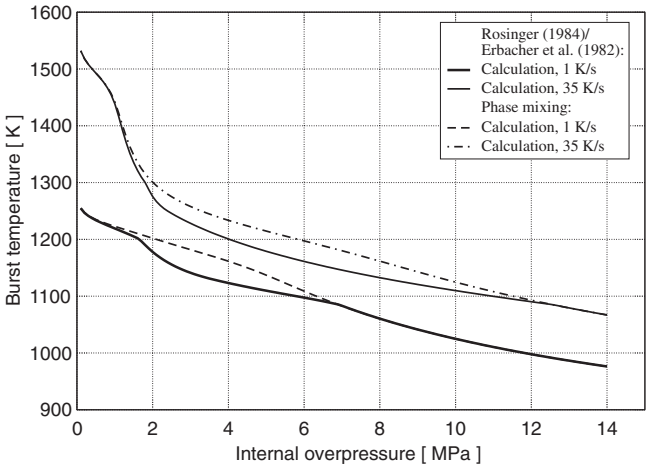

(b)

Fig. 9 Calculated (a) burst strain versus burst temperature and (b) burst temperature versus rod internal overpressure at two different heating rates, 1 and 35 K s^{-1}. Solid lines: Creep rate and burst stress are according to correlations listed in Tables 1 and 3, respectively. Broken lines: Creep rate and burst stress in the two-phase coexistence ($\alpha + \beta$) region are calculated by combining the single-phase creep rates of Ref. 5) and burst stress of Ref. 4) according to Eqs. (14) and (15), respectively.

azimuthal temperature difference around the circumference of the cladding tube. Small azimuthal temperature gradients (few degrees) cause a relatively homogeneous decrease in cladding wall thickness around its circumference, therefore leading to relatively large burst strains. On the other hand, large azimuthal temperature gradients, which may occur during the course of deformation, lead to a localised reduction in wall thickness on the hotter part of the cladding tube circumference, thus resulting in small burst strains. As such, the magnitude of the azimuthal temperature gradient around the tube's circumference is an important factor affecting cladding burst strain.

3. Parametric Study

In the computations presented in the foregoing subsections, the creep rate and burst stress of cladding were calculated according to the correlations of Rosinger[5] and Erbacher *et al.*,[4] Tables 1 and 3, respectively. Since in these correlations, the behaviours in the two-phase coexistence ($\alpha + \beta$) are constructed in an *ad hoc* fashion, *i.e.*, using parameter fitting on a limited set of data and conditions, their wider applicability is questionable (see Sec. IV). Other workers have recommended phase mixing rules for calculating the creep rate[11] and burst stress[12] in the two-phase coexistence ($\alpha + \beta$) domain of Zr alloys. Hence, it is worthwhile to utilise the output of our phase transition model, that is, the fraction of the β-phase as a function of time (temperature), to calculate the creep rate and the burst stress in the ($\alpha + \beta$) domain, through Eqs. (14) and (15), and thereafter, compute the burst strain as a function of burst temperature and internal rod overpressure, and compare the results with those predicted using single creep and burst correlations (with no phase mixing in the two-phase coexistence domain) given in Tables 1 and 3.

Figure 9(a) illustrates the difference between the two methods of computation regarding the prediction of burst

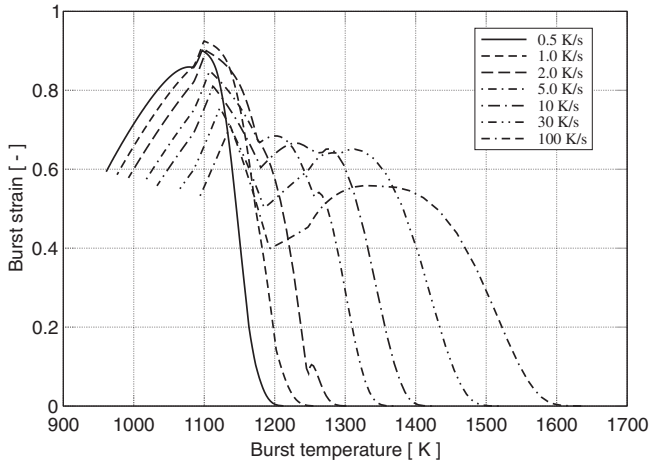

(a)

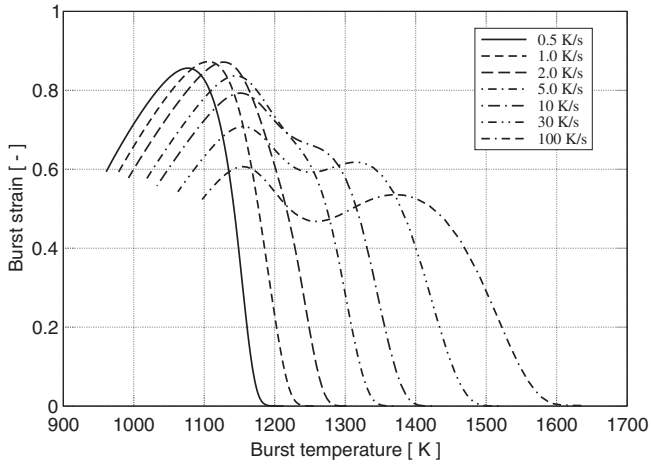

(b)

Fig. 10 Calculated burst strain versus burst temperature for various heating rates. Each curve covers Zircaloy-4 tube internal overpressures in the range of 0.1 to 14 MPa in steps of 0.1 MPa. (a) Creep rate and burst stress are according to Tables 1 and 3, respectively. (b) Creep rate and burst stress in the two-phase coexistence ($\alpha + \beta$) region are calculated by combining the single-phase creep rates of Ref. 5) and burst stress of Ref. 4) according to Eqs. (14) and (15), respectively.

strain-temperature behaviour for heating rates of 1 and 35 K s^{-1}. The assumptions for the computations are the same as those used to calculate the lines in Fig. 7. It is seen that in the case of 1 K s^{-1}, the difference between the two procedures is negligible, while at 35 K s^{-1}, the two methods differ in the ($\alpha + \beta$) domain, 1,100–1,250 K. Nevertheless, the difference between the results is within the experimental scatter of the data (*cf.* Fig. 7). The corresponding calculations for cladding burst temperature versus internal rod overpressure are shown in Fig. 9(b).

Finally, **Figs. 10**(a)–10(b) depict computations of burst strain versus burst temperature as a function of heating rate for the two aforementioned procedures. It is seen that the phase mixing method smoothens the anomalies seen in Fig. 10(a), which are artifacts of the discontinuities in the creep rate equation of Rosinger[5] and the burst criterion of Erbacher *et al.*,[4] Tables 1 and 3, while keeping the trends

Table 4 Calculated burst data at a heating rate of 10 K s^{-1} *vs.* Zircaloy-4 tube internal overpressure

Overpressure MPa	Time s	Temperature K	Hoop strain %	Hoop stress MPa
1	44.5	1,345	29.8	12.5
2	34.2	1,242	66.0	51.8
3	29.9	1,199	63.7	74.2
4	27.3	1,173	63.1	97.7
5	25.3	1,153	70.1	140.5
6	23.7	1,137	75.0	186.1
7	22.2	1,122	78.7	233.6
8	21.0	1,110	79.9	273.2
9	19.8	1,098	74.6	276.6
10	18.7	1,087	69.9	279.8
11	17.2	1,072	65.9	284.1
12	15.7	1,057	62.3	288.3
13	14.5	1,045	58.9	292.0
14	13.3	1,033	55.8	295.4

correctly. **Table 4** lists the burst data as a function of pressure for the heating rate of 10 K s^{-1} corresponding to Fig. 10(a). The diagrams show the prominent role of heating rate on burst strain. In the α-phase, the burst strain decreases with increasing heating rate, whereas in the mixed ($\alpha + \beta$) domain and β-phase, the situation is more complex. For example, at 1,300 K (β-phase), the burst strain increases with increasing rate up to a heating rate of 10 K s^{-1}, then declines consecutively at 30 and 100 K s^{-1}. Also, the higher heating rates shift the burst temperatures to higher values for burst strains below 50%.

IV. Discussion

We have presented an integrated model for the rupture of zirconium alloy fuel claddings in a postulated loss-of-coolant accident in nuclear power reactors. We have solved the kinetic equations for phase transformation, creep, and oxidation of cladding in a unified fashion, where the latter two coupled equations were solved simultaneously, but separately from the phase transformation kinetics.

In the calculations presented in Sec. III, we have used material parameters from the literature for oxidation, creep rate, and burst stress of Zircaloy-4 cladding applicable to LOCA conditions. For the latter two quantities, we have used correlations in α-Zr and β-Zr separately, while for the two-phase coexistence ($\alpha + \beta$)-Zr, we have either utilised explicit correlations for the region or employed mixing rules according to relations (14) and (15). The latter was done by combining the correlations in the single-phase regions with the output of the phase transformation model described by Eq. (1) and the mixing rules. The use of such recipes to obtain the creep rate and burst stress in the two-phase coexistence region must be supported by experimental data. For the burst stress parameters, the data presented and evaluated in Refs. 12) and 13) endorse the use of relation (15). On the other hand, the situation for creep rate is quite different. Rosinger[5] offered an empirical correlation for the creep rate of Zircaloy-4 in ($\alpha + \beta$) domain, which is presented in

Table 1. The values for A_z, Q, and n, listed in Table 1, were derived from measurements of the uniaxial steady-state creep rate of Zircaloy-4 fuel cladding.[23] More specifically, these values are for α-Zr, from 823 to 1,085 K, for $(\alpha + \beta)$-Zr, from 1,085 to 1,248 K, and for β-Zr, from 1,248 to 1,873 K.

We believe, at the fundamental level, that the main uncertainty in modelling arises from the creep behaviour of Zircaloy in the two-phase coexistence $(\alpha + \beta)$ domain. The other uncertainties, such as oxidation modelling and azimuthal temperature gradients, although appreciable, can be reduced by more detailed modelling efforts and/or more refined and controlled tests. On the other hand, our understanding of the mechanism of creep in the $(\alpha + \beta)$ domain remains speculative as has been proven by the recent work of Kaddour *et al.*[15] It has been noted by Kaddour *et al.*[15] that Zircaloy-4 in the α domain ($T < 1{,}023$ K) experimental data exhibits two creep regimes: At low stresses ($\sigma < 15$ MPa), the creep stress exponent is $n \approx 1$, *cf.* Eqs. (3)–(4), suggesting that the deformation mechanism could be "diffusional creep;" while at higher stresses ($\sigma > 15$ MPa), the deformation mechanism is most likely "dislocation-climb-induced creep," with n in the range of 4–5; see Ref. 30) for a review of creep mechanisms. In the β domain, Kaddour *et al.*[15] observed only one regime, *i.e.*, "dislocation-climb-induced creep," *cf.* Table 2. In the two-phase coexistence $(\alpha + \beta)$ domain, however, the creep behaviour is more complex, and as such, no simple creep law has been established. Kaddour *et al.*[15] have observed that for very low applied stresses (1–2 MPa), strain rates in the $(\alpha + \beta)$ domain are substantially higher than those measured in the single-phase domains including the high-temperature region of the β-phase. The estimated stress exponent $n \approx 1.5$ by Kaddour *et al.*[15] suggests that, in the $(\alpha + \beta)$ domain, the deformation mechanism could be controlled by "interphase interface sliding," which is the hallmark of superplasticity. Superplasticity is the tendency of a polycrystalline to deform extensively at elevated temperatures ($T > 0.5T_m$), prior to rupture, where T_m is the melting point of the solid.[30,31] One of us[32] has recently evaluated the creep rate data of Kaddour *et al.*[15] on Zr-1 wt%Nb alloy by using the mixing rule given by Eq. (14), but the outcome in the $(\alpha + \beta)$ domain was unsatisfactory.

As has been pointed out by Mukherjee,[31] the three main requirements for superplastic behaviour are (i) fine (less than roughly 10 μm) and equiaxed grain size that is fairly stable during deformation, (ii) a temperature that is higher than about half of the melting point of the solid, and (iii) a strain rate that is normally not too high (less than 0.001 s^{-1}) or not too low (more than 10^{-6} s^{-1}). These requirements are satisfied by nuclear-grade Zircaloy materials in the $(\alpha + \beta)$ domain. For example, Kaddour *et al.*'s[15] Zircaloy-4 samples had equiaxed grains with a mean size of 5 μm.

Simple constitutive relations of the form defined by Eqs. (3)–(4) with parameters based on fitting a limited set of data seem to be inadequate for describing the superplastic behaviour in the two-phase coexistence $(\alpha + \beta)$ domain of zirconium-based alloys. A more general relation for the steady-state creep rate is given by[31]

$$\frac{d\varepsilon}{dt} = \frac{ADGb}{k_B T}\left(\frac{b}{d}\right)^p \left(\frac{\sigma}{G}\right)^n. \tag{16}$$

Here, A is a material-dependent (dimensionless) constant, D is the appropriate diffusion coefficient, $D = D_0 \exp(-Q/k_B T)$, D_0 is the frequency factor, Q the activation energy of diffusion, k_B the Boltzmann constant, G the shear modulus, b the magnitude of the Burgers vector, d the grain size, and p the inverse grain size exponent. In this setting, Spingarn and Nix[33] note that at small stresses (and strains), the exponents in relation (16) are given by $p = 3$ and $n = 1$, which describe the diffusional creep. At large stresses, however, $p = 1$ and $n = 5$, which characterise creep that is controlled by edge dislocations. Spingarn and Nix[33] suggest that the transition from $n = 1$ to $n = 5$ behaviour corresponds to the superplastic domain. But no specific constitutive relation in the form of Eq. (16) is provided for this domain.

Garde *et al.*[34] have investigated the uniaxial stress-strain behaviour of Zircaloy-4 at temperatures of 973 to 1,673 K. They observed a superplastic peak at 1,123 K. At 1,123 to 1,173 K, they found that at low strain rates ($< 10^{-4}$ s^{-1}), the predominant mechanism of superplasticity was grain boundary sliding, whereas at high strain rates ($> 10^{-4}$ s^{-1}), dislocation creep was prevailing. In particular, they found that for Zircaloy-4 with an equiaxed grain structure, the value of the exponent n very much depended on the strain rate in the $(\alpha + \beta)$-Zr. For example, at 1,123 K, $n \approx 1.25$ for a low strain rate of $\dot{\varepsilon} \approx 3 \times 0^{-6}$ s^{-1}, then increasing continuously to $n \approx 5$ as the strain rate was increased to $\dot{\varepsilon} \approx 2 \times 10^{-3}$ s^{-1}. For Zircaloy-4 with a basketweave (acicular) grain structure, the variation in the exponent was from $n \approx 3.3$ to $n \approx 5$ in the same span of strain rate.

Rosinger *et al.*[23] by curve fitting various experimental data on the creep of Zircaloy-4 in the mixed phase $(\alpha + \beta)$ domain to Eq. (3) deduced an average value of $n \approx 1.88$ for $\dot{\varepsilon} < 3 \times 10^{-3}$ s^{-1}. Later, Rosinger[5] changed this value to $n \approx 2.33$, as listed in Table 1 (at the same time, he changed the values for A_z and Q, so the overall outputs were similar). To deduce the parameters for the creep law in the superplasticity region in this manner is very simplistic, so is the phase mixing method described by relation (14) to combine the creep mechanisms in single-phase domains. Rosinger *et al.*[23] noted that, due to "the dramatic change in stress exponent (of the creep rate), it is not possible, unambiguously, to identify the mechanism operating in the mixed $(\alpha + \beta)$-phase. Additional experimental effort is required to determine the exact nature of creep equations with their limits of applicability and to identify the mechanisms controlling the creep in the mixed $(\alpha + \beta)$-phase." In other words, a constitutive relation for creep in this region is missing.

To find out the difference between the phase mixing method and that recommended by Rosinger,[5] we have compared computations of creep strain as a function of temperature (time) for a heating rate of 10 K s^{-1} using the choice of parameters given in Table 1 for $(\alpha + \beta)$-Zr and the phase mixing method given by relation (14). The results are presented in **Fig. 11**. A significant difference in strain behaviour between the two methods of calculation is seen in the $(\alpha +$

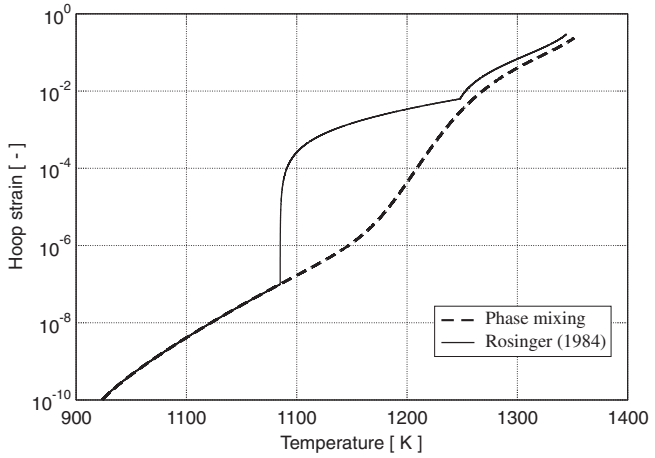

Fig. 11 Hoop strain of Zircaloy-4 cladding due to creep versus temperature during the transient at a rod internal overpressure of 1 MPa. Phase mixing (dashed line) refers to the rule per Eq. (14) as in Fig. 4, while the solid line is the outcome of the parameter designations in Table 1 for $(\alpha + \beta)$-Zr.[5)]

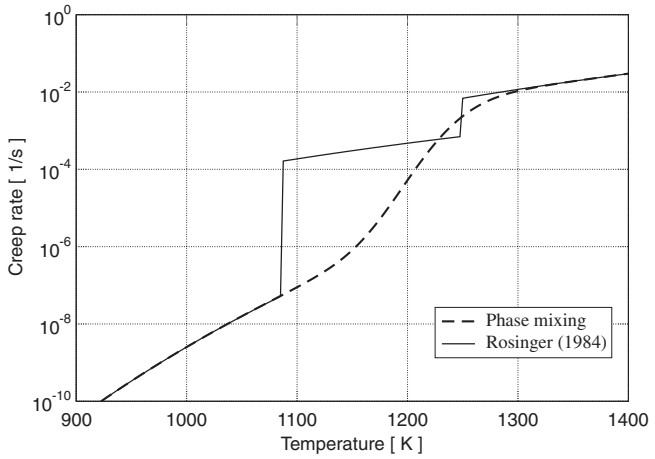

Fig. 12 Creep rate $\dot{\varepsilon}_\theta$ of Zircaloy-4 versus temperature during the transient at a rod internal overpressure of 1 MPa. Phase mixing (dashed line) refers to the rule per Eq. (14), while the solid line is the outcome of the parameter designations in Table 1 for $(\alpha + \beta)$-Zr.[5)]

β) region. To elucidate further, we have plotted the corresponding creep rates obtained from the two methods in **Fig. 12**. Despite the marked difference, the overall impact on the rupture strain versus rupture temperature is not as dramatic, *cf.* Fig. 10.

In the present note, we did not make an in-depth analysis of creep behaviour in the two-phase coexistence $(\alpha + \beta)$ domain. This is a topic for a separate study. But comparing the works of Rosinger *et al.*[23)] with that of Kaddour *et al.*,[15)] it is ironic that not much progress in understanding of the phenomenon has been gained in the span of 25 years. Our limited analysis indicates that the present models for creep laws cannot be applied without extensive parameter fitting in the two-phase coexistence $(\alpha + \beta)$ regime, and the resulting correlations would probably have a restricted applicability.

As discussed in our previous paper,[3)] oxygen concentration affects the phase transition temperature in Zr alloys, and it is expected to have an impact on the kinetics of phase transition. Thus, strictly speaking, Eq. (1) should also depend on oxygen concentration. Experimental data, however, are required for a quantitative modelling of this phenomenon. When such data become available, an extension of our model to account for this effect is straightforward. Then, the three coupled differential equations will be solved simultaneously.

The Zircaloy-4 cladding oxidation model used in our calculations assumes a uniform oxygen uptake across the cladding wall. This is based on the empirical correlation for the oxygen uptake versus time and temperature obtained from experiments of Leistikow *et al.* (1978) cited in Ref. 4). More precisely, the correlation is expressed as $\varrho = 0.724\sqrt{t}\,e^{-10481/T}$, where ϱ is the oxygen uptake in g/cm^2, t the exposure time in second, and T the oxidation temperature in kelvin. This correlation was found from isothermal steam oxidation tests made on Zircaloy-4 cladding within a temperature interval of 700 to 1,300°C. It has been noted by Erbacher *et al.*[4)] that this correlation provides a good approximation to oxygen uptake for the type of tests we have analyzed here. We are, however, aware of many studies that show that the oxygen concentration of the oxidized Zircaloy cladding varies significantly across the cladding wall, for example, Ref. 35). Nevertheless, the use of an effective or average oxygen concentration gives a fair approximation of the oxygen effect, as discussed in earlier evaluations of experimental data.[5)] The empirical correlations used to account for the effect of oxidation on cladding creep, *cf.* Eqs. (4)–(5), and the cladding rupture stress, *cf.* Eqs. (11)–(12), are all based on a uniform concentration of oxygen in sample cladding tubes. More elaborate oxidation models and/or correlations could be introduced, but that would require accurate experimental data, which specify the creep and burst as a function of local oxygen concentration.

The cladding tube test samples in the three data sets, used for comparison with our model calculations, were under various degrees of azimuthal temperature variations during the experiments. More specifically, the azimuthal temperature variations (ΔT) of the tests reported by Erbacher *et al.*,[4)] Erbacher and Leistikow,[28)] and Karb *et al.*[27)] were $\Delta T < 15$ K, $20 < \Delta T < 70$ K, and $0 < \Delta T < 80$ K, respectively. The burst test data provided by Erbacher *et al.*[4)] are the most appropriate among the three data sets for our comparison, since the influence of azimuthal temperature variation is least for this data set ($\Delta T < 15$ K). Our calculations of the cladding burst strain, employing a best estimate (average) type of correlation for burst stress (Table 3), show an overall good agreement for this data set (see Fig. 7(b)). The other two data sets, having generally larger azimuthal temperature variations, fall mostly below the calculated burst strains, thus indicating the influence of azimuthal temperature variation (Fig. 7(b)). As noted by Rosinger,[5)] the experimental data on burst strain versus burst temperature commonly show very large scatter. Some of the scatter is due to the lack of sufficient data characterization,

e.g., anisotropy, but mostly due to experimental uncertainty including the effect of azimuthal temperature variation. Varty and Rosinger[36] carried out a sensitivity study for $\Delta T = 10 \pm 10\,\mathrm{K}$, which showed that the burst strain varies from its nominal value of 0.73 by ± 0.36. Meaning that burst strain values could vary from 1.09 to 0.37 just due to the variation in experimental conditions. In spite of this complication, the burst model presented here has been developed with the intention for use also in nonsymmetrical tube deformation encountered in the case of azimuthal temperature variations. In this situation, the burst criterion must be applied locally. In addition, the model could be employed for any pressure and temperature history in the range of its validity.

The impact of rod internal pressure on cladding rupture limit was evaluated briefly here (Table 4). Increasing the rod internal pressure shortens the time to rupture and lowers the rupture temperature. If the differential pressure is varying during the transient, Eq. (7) can be scaled linearly with pressure by a factor p/p_0, where p_0 is the initial pressure and p the current pressure. The computational method described here can readily be implemented in a transient fuel rod modelling code for assessing the cladding rupture under LOCA.[37]

V. Conclusions

A unified computer model for the rupture of fuel cladding during loss-of-coolant conditions has been presented. The model consists of interconnected modules for Zircaloy phase transformation, creep, oxidation, and rupture under LOCA conditions. The main part of the model uncertainty at the fundamental level is the treatment of creep deformation in the two-phase coexistence ($\alpha + \beta$) domain of the alloy, for which neither the existing correlations nor the phase mixing rules seem to be appropriate. The modelling of creep rate in the two-phase domain of zirconium alloys requires further investigation.

Acknowledgements

We would like to thank the anonymous reviewers for their helpful comments. The work was supported by the Swedish Radiation Safety Authority (SSM) under contract number SSM 2008/139.

References

1) P. D. Parsons, E. D. Hindle, C. A. Mann, *The Deformation, Oxidation and Embrittlement of PWR Fuel Cladding in a Loss-of-Coolant Accident*, CSNI 129, OECD Nuclear Energy Agency, Paris, France (1986).
2) K. Pettersson, *Nuclear Fuel Behaviour in Loss-of-Coolant (LOCA) Conditions*, NEA No. 6846, OECD Nuclear Energy Agency, Issy-les-Moulineaux, France (2009).
3) A. R. Massih, "Transformation kinetics of zirconium alloys under non-isothermal conditions," *J. Nucl. Mater.*, **384**, 330–335 (2009).
4) F. J. Erbacher, H. J. Neitzel, H. Rosinger, H. Schmidt, K. Wiehr, "Burst criterion of Zircaloy fuel claddings in a loss-of-coolant accident," *Zirconium in the Nuclear Industry: Fifth Conf.*, ASTM STP 754, American Society for Testing and Materials, 271–283 (1982).
5) H. E. Rosinger, "A model to predict the failure of Zircaloy-4 fuel sheathing during postulated LOCA conditions," *J. Nucl. Mater.*, **120**, 41–54 (1984).
6) C. Lemaignan, A. T. Motta, "Zirconium alloys in nuclear applications," *Nuclear Materials*, R. W. Cahn, P. Haasen, E. J. Kramer (Eds.), Series: Materials Science and Technology, Vol. 10B, VCH, Weinheim, Germany, 1–51 (1994).
7) A. Miquet, D. Charquet, C. H. Allibert, "Solid state phase equilibria of Zircaloy-4 in the temperature range 750–1050°C," *J. Nucl. Mater.*, **105**, 132–141 (1982).
8) N. V. Bangaru, R. A. Busch, J. H. Schemel, "Effects of beta quenching on the microstructure and corrosion of Zircaloys," *Zirconium in the Nuclear Industry: Seventh Int. Symp.*, ASTM STP 939, American Society for Testing and Materials, 341–363 (1987).
9) A. Miquet, D. Charquet, C. Michaut, C. H. Allibert, "Effect of Cr, Sn and O contents on the solid state phase boundary temperature of Zircaloy-4," *J. Nucl. Mater.*, **105**, 142–148 (1982).
10) H. M. Chung, T. F. Kassner, "Pseudobinary Zircaloy-oxygen phase diagram," *J. Nucl. Mater.*, **84**, 327–339 (1979).
11) P. Van Uffelen, C. Győri, A. Schubert, J. van de Laar, Z. Hózer, G. Spykman, "Extending the application range of a fuel performance code from normal operating to design basis accident conditions," *J. Nucl. Mater.*, **383**, 137–143 (2008).
12) T. Forgeron, J. C. Brachet, F. Barcelo, A. Castaing, J. Hivroz, J. P. Mardon, C. Bernaudat, "Experiment and modeling of advanced fuel rod cladding behavior under LOCA conditions: Alpha-beta phase transformation kinetics and EDGAR methodology," *Zirconium in the Nuclear Industry: Twelfth Int. Symp.*, ASTM STP 1354, American Society for Testing and Materials, 256–278 (2000).
13) J. C. Brachet, L. Portier, T. Forgeron, J. Hivroz, D. Hamon, T. Guilbert, T. Bredel, P. Yvon, J.-P. Mardon, P. Jacques, "Influence of hydrogen content on the α/β phase transformation temperatures and on the thermal-mechanical behavior of Zy-4, M4 (ZrSnFeV), and M5™ (ZrNbO) alloys during the first phase of LOCA transient," *Zirconium in the Nuclear Industry: Thirteenth Int. Symp.*, ASTM STP 1423, American Society for Testing and Materials, 673–701 (2002).
14) A. R. Massih, L. O. Jernkvist, "Transformation kinetics of alloys under non-isothermal conditions," *Modelling Simul. Mater. Sci. Eng.*, **17**, 055002(15pp) (2009).
15) D. Kaddour, S. Frechinet, A. F. Gourgues, J. C. Brachet, L. Portier, A. Pineau, "Experimental determination of creep properties of zirconium alloys together with phase transformation," *Scripta Mater.*, **51**, 515–519 (2004).
16) B. Burton, A. T. Donaldson, G. L. Reynolds, "Interaction of oxidation and creep in Zircaloy-2," *Zirconium in the Nuclear Industry: Fourth Conf.*, ASTM STP 681, American Society for Testing and Materials, 561–585 (1979).
17) R. Hill, "A theory of yielding and plastic flow of anisotropic materials," *Proc. R. Soc. A*, **193**, 281–297 (1948).
18) H. J. Neitzel, H. E. Rosinger, *The Development of a Burst Criterion for Zircaloy Fuel Cladding under LOCA Conditions*, AECL-6420, Atomic Energy of Canada Limited (1980).
19) S. Sagat, H. E. Sills, J. A. Walsworth, "Deformation and failure of Zircaloy fuel sheets under LOCA conditions," *Zirconium in the Nuclear Industry: Sixth Int. Symp.*, ASTM STP 824, American Society for Testing and Materials, 709–733 (1984).

20) J. R. Matthews, "The effect of anisotropy on the ballooning of Zircaloy cladding," *Nucl. Eng. Des.*, **77**, 87–95 (1984).
21) R. S. W. Shewfelt, "The ballooning of fuel cladding tubes: Theory and experiment," *Res Mechanica*, **25**, 261–294 (1988).
22) K. Nuttall, "Superplasticity in the Zr-2.5%Nb alloy," *Scripta Metall.*, **10**, 835–840 (1976).
23) H. E. Rosinger, P. C. Bera, W. R. Clendening,"Steady-state creep of Zircaloy-4 fuel cladding from 940 to 1873 K," *J. Nucl. Mater.*, **82**, 286–297 (1979).
24) E. N. Pirogov, M. I. Alymov, L. L. Artyukhina, "Creep of N1 alloy within the region of polymorphic transformation," *Atomic Energy*, **65**, 864–866 (1989) (translated from *Atomnaya Energiya*, **65**, 293–294 (1988)).
25) W. H. Press, S. A. Teukolsky, W. T. Vetterling, B. P. Flannery, *Numerical Recipes in FORTRAN*, Second Edition, Cambridge University Press, Cambridge, Chap. 16 (1992).
26) F. J. Erbacher, H. J. Neitzel, K. Wiehr, "Studies on Zircaloy fuel clad ballooning in a loss-of-coolant accident—Results of burst tests with indirectly heated fuel simulators," *Zirconium in the Nuclear Industry: Fourth Conf.*, ASTM STP 681, American Society for Testing and Materials, 429–446 (1979).
27) E. H. Karb, L. Sepold, P. Hofmann, C. Petersen, G. Schanz, H. Zimmermann, "LWR fuel rod behavior during reactor tests under loss-of-coolant conditions: Results of the FR2 in-pile tests," *J. Nucl. Mater.*, **107**, 55–77 (1982).
28) F. J. Erbacher, S. Leistikow, "Zircaloy fuel cladding behavior in a loss-of-coolant accident: A review," *Zirconium in the Nuclear Industry: Seventh Int. Symp.*, ASTM STP 939, American Society for Testing and Materials, 451–488 (1987).
29) E. H. Karb, M. Prüßmann, L. Sepold, P. Hofmann, G. Schanz, *LWR Fuel Rod Behavior in the FR2 In-Pile Tests Simulating the Heatup Phase of a LOCA*, KfK 3346, Kernforschungszentrum Karlsruhe, Germany (1983).
30) M. E. Kassner, *Fundamentals of Creep in Metals and Alloys*, Elsevier, Amsterdam, The Netherlands, Chap. 6 (2009).
31) A. K. Mukherjee, "Superplasticity in metals, ceramics and intermetallics," *Plastic Deformation and Fracture of Materials*, R. W. Cahn, P. Haasen, E. J. Kramer (Eds.), Series: Materials Science and Technology, Vol. 6, VCH, Weinheim, Germany, 407–460 (1993).
32) A. R. Massih, *A Model for Analysis of Zr Alloy Fuel Cladding Behaviour under LOCA Conditions*, TR08-007v1, Quantum Technologies AB, Uppsala, Sweden (2009) (to be issued by the Swedish Radiation Safety Authority).
33) J. R. Spingarn, W. D. Nix, "A model for creep based on the climb at grain boundaries," *Acta Metall.*, **27**, 171–177 (1979).
34) A. M. Garde, H. M. Chung, T. F. Kassner, "Micrograin superplasticity in Zircaloy at 850°C," *Acta Metall.*, **26**, 153–166 (1978).
35) R. E. Pawel, R. A. Perkins, R. A. McKee, J. V. Cathcart, G. J. Yurek, R. E. Druschel, "Diffusion of oxidation in beta-Zircaloy and high temperature Zircaloy-steam oxidation," *Zirconium in the Nuclear Industry*, ASTM STP 633, American Society for Testing and Materials, 119–133 (1977).
36) R. L. Varty, H. E. Rosinger, *Comparison of Sheath Failure Model with Published Experimental Data*, AECL-6806, Atomic Energy of Canada Limited, Pinawa, Manitoba, Canada (1982).
37) T. Manngård, *Implementation of Cladding Material Models in FRAPTRAN-1.3 for LOCA Application*, TR09-002v1, Quantum Technologies AB, Uppsala, Sweden (2009) (to be issued by the Swedish Radiation Safety Authority).